

# OctGPT: Octree-based Multiscale Autoregressive Models for 3D Shape Generation

SI-TONG WEI, Peking University, China  
 RUI-HUAN WANG, Peking University, China  
 CHUAN-ZHI ZHOU, Peking University, China  
 BAOQUAN CHEN, Peking University, China  
 PENG-SHUAI WANG\*, Peking University, China

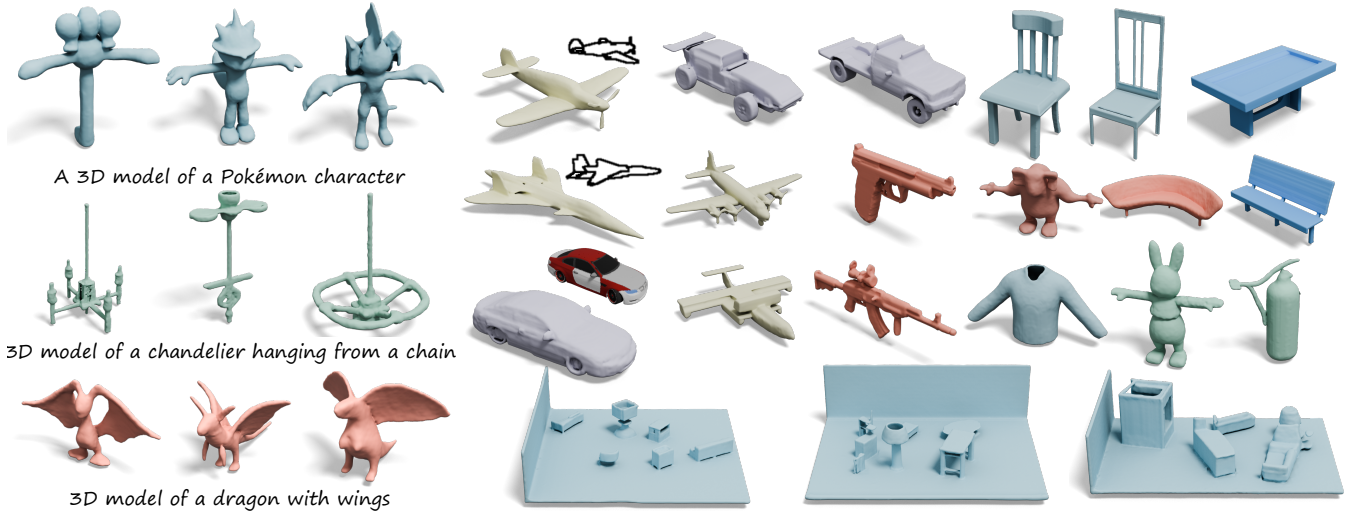


Fig. 1. OctGPT generates high-quality 3D shapes in diverse scenarios, including unconditional, category-, text- and image-conditioned generation, as well as large-scale scene synthesis.

Autoregressive models have achieved remarkable success across various domains, yet their performance in 3D shape generation lags significantly behind that of diffusion models. In this paper, we introduce OctGPT, a novel multiscale autoregressive model for 3D shape generation that dramatically improves the efficiency and performance of prior 3D autoregressive approaches, while rivaling or surpassing state-of-the-art diffusion models. Our method employs a serialized octree representation to efficiently capture the hierarchical and spatial structures of 3D shapes. Coarse geometry is encoded via octree structures, while fine-grained details are represented by binary tokens generated using a vector quantized variational autoencoder (VQVAE), transforming 3D shapes into compact *multiscale binary sequences* suitable for autoregressive prediction. To address the computational challenges of handling long sequences, we incorporate octree-based transformers enhanced with 3D rotary positional encodings, scale-specific embeddings, and token-parallel generation schemes. These innovations reduce training time by 13 folds and generation time by 69 folds, enabling the efficient training of high-resolution 3D shapes, e.g.,  $1024^3$ , on just four NVIDIA 4090 GPUs only within days. OctGPT showcases exceptional versatility across various

tasks, including text-, sketch-, and image-conditioned generation, as well as scene-level synthesis involving multiple objects. Extensive experiments demonstrate that OctGPT accelerates convergence and improves generation quality over prior autoregressive methods, offering a new paradigm for high-quality, scalable 3D content creation. *Our code and trained models are available at <https://github.com/octree-nn/octgpt>.*

CCS Concepts: • **Computing methodologies** → **Shape modeling; Neural networks.**

Additional Key Words and Phrases: Octree, Transformers, Autoregressive Models, GPT, 3D Generation, Scene Generation

## 1 INTRODUCTION

3D content creation has experienced rapid advancements in recent years, driven largely by diffusion models [Cheng et al. 2023; Chou et al. 2023; Gupta et al. 2023; Hui et al. 2022; Li et al. 2023; Ren et al. 2024; Zhang et al. 2023, 2024b; Zheng et al. 2023]. Meanwhile, autoregressive models have achieved remarkable success across various domains, including large language models [Brown et al. 2020; Ouyang et al. 2022; Touvron et al. 2023], image generation [Sun et al. 2024; Tian et al. 2024], and large multimodal models [OpenAI 2023; Wang et al. 2024b]. Despite these successes, the performance of autoregressive models in 3D shape generation continues to lag behind that of diffusion models. Exploring the potential of autoregressive models in

\*Corresponding author.

Authors' addresses: Si-Tong Wei, Wangxuan Institute of Computer Technology, Peking University, China, weisitong@pku.edu.cn; Rui-Huan Wang, Peking University, China, wangrs@pku.edu.cn; Chuan-Zhi Zhou, Peking University, China, 2200011057@stu.pku.edu.cn; Baoquan Chen, Peking University, China, baoquan@pku.edu.cn; Peng-Shuai Wang, Wangxuan Institute of Computer Technology, Peking University, China, wangps@hotmail.com.

3D content creation may unlock new possibilities for improving the quality, diversity, and scalability of generated 3D shapes, ultimately paving the way for the development of general multimodal models.

Autoregressive models operate by predicting the next token based on previous tokens using transformers [Vaswani et al. 2017]. While conceptually straightforward, applying autoregressive models to 3D shape generation presents several challenges. The first challenge stems from the fact that autoregressive models need to define a sequential order for tokens, which does not naturally exist for 3D shapes. Previous approaches often flatten 3D tokens into 1D sequences using rasterization orders based on 3D positions [Chen et al. 2024a; Siddiqui et al. 2024; Yan et al. 2022; Zhang et al. 2022]. However, such approaches overlook the hierarchical structure and spatial locality inherent to 3D shapes, leading to slower convergence and suboptimal generation quality. Another challenge lies in that 3D shapes require a large number of tokens to capture the complex geometry and topology, which makes both the training and inference processes computationally intensive. To address this, prior works have explored compact mesh-based representations [Chen et al. 2024a; Nash et al. 2020; Siddiqui et al. 2024] and low-dimensional tokenization schemes [Mittal et al. 2022; Yan et al. 2022; Zhang et al. 2022], reducing the token count to approximately 1k. Despite these efforts, these methods still face limitations in expressiveness and struggle to produce high-quality 3D shapes with fine-grained details.

In this paper, we present an efficient and scalable autoregressive model for 3D shape generation with a novel serialized octree representation, achieving quality and scalability that even surpass state-of-the-art diffusion models. Our key observation is that octrees inherently capture the hierarchical structure of 3D shapes while providing a locality-preserving order suitable for autoregressive prediction, as octree nodes at each depth are sorted in z-order by construction [Wang 2023; Zhou et al. 2011]. We convert input shapes into octrees by recursively splitting nodes to a specified depth or resolution. We regard the node-splitting status as a 0/1 binary signal and concatenate these signals across each octree depth from coarse to fine, forming a 1D sequence. While the octree structure effectively captures coarse geometry, it lacks fine-grained geometric details. To address this, we supplement the octree with additional binary tokens defined at the finest octree nodes, generated by a vector quantized variational autoencoder (VQVAE) [van den Oord et al. 2017] that is built on octree-based neural networks [Wang et al. 2017, 2022], using binary spherical quantization [Zhao et al. 2024]. These binary tokens are concatenated with the binary splitting signals to form the final input sequence for the autoregressive model. The autoregressive model is trained to predict the binary sequence through a series of binary classification tasks. During inference, the predictions are assembled to reconstruct the octree structure, from coarse to fine, along with the binary tokens at the finest octree nodes, which are decoded into continuous signed distance fields (SDFs) by the decoder of the VQVAE. The SDFs are subsequently converted to meshes using the marching cubes algorithm [Lorensen and Cline 1987] as the final output.

In contrast to previous autoregressive models that directly predict 3D coordinates [Chen et al. 2024a; Siddiqui et al. 2024; Yan et al. 2022; Zhang et al. 2022], our approach decomposes the generation

task into a series of simpler binary classification tasks. This methodology is inspired by the chain-of-thought paradigm [Wei et al. 2022], which improves the reasoning capabilities of large language models by breaking down complex reasoning into a sequence of intermediate steps. By adopting this approach, we achieve significantly faster convergence and higher generation quality compared to direct coordinate prediction. For instance, in one of our experiments, our method generated high-quality 3D shapes after just 10 epochs of training, whereas the coordinate prediction approach failed to produce satisfactory results even after 100 epochs.

The token length of our serialized octree representation can exceed 50k, posing a challenge for naive autoregressive models, which have quadratic time complexity. To circumvent this issue, we adapt octree-based transformers [Wang 2023] with several improvements that reduce time complexity to linear, achieving a speedup of 13 folds. As a result, our model can be trained on four NVIDIA 4090 GPUs with 24GB of memory. We further incorporate the parallel token prediction scheme proposed by [Li et al. 2024], accelerating the generation process by 69 folds and enabling the generation of high-resolution 3D shapes with resolution  $1024^3$  in under 30 seconds on a single NVIDIA 4090 GPU. Additionally, we extend rotary positional encodings [Wang 2023] to 3D and introduce scale-specific positional encodings for each token, enhancing the model’s ability to distinguish multiscale binary signals in the serialized octree representation. As our training and prediction process is in a GPT-like style [Brown et al. 2020], we name our model OctGPT.

We evaluate the effectiveness of our OctGPT across various 3D shape generation tasks, including shape generation on ShapeNet [Chang et al. 2015] and Objaverse [Deitke et al. 2023], text- or image-conditioned generation, and large-scale scene generation. The generation results showcased in Fig. 1 highlight the high-quality 3D shapes at a resolution of  $1024^3$  produced in diverse scenarios. Quantitative evaluations demonstrate that OctGPT significantly outperforms previous 3D autoregressive models [Chen et al. 2024a; Mittal et al. 2022; Zhang et al. 2022] in terms of generation quality, diversity, and scalability, and even surpasses state-of-the-art 3D diffusion models in certain cases. OctGPT offers a new paradigm for 3D content creation, distinct from diffusion models. We believe it can inspire further exploration within the 3D generation community and promote the development of multimodal models through alignment or fine-tuning from large language and image models [Liu et al. 2024]. In summary, our main contributions are as follows:

- We propose a 3D autoregressive model trained on serialized multiscale binary tokens induced by octrees for 3D shape generation, significantly improving the efficiency and scalability of 3D autoregressive models compared to previous works.
- We extend octree-based transformers to handle multiscale octree nodes and adapt a parallel token prediction scheme, accelerating training speed by 13 folds and generation speed by 69 folds.
- We demonstrate that autoregressive models can be effectively applied to 3D shape and scene generation, achieving competitive results with state-of-the-art diffusion models, while requiring only 3 days of training on 4 Nvidia 4090 GPUs.

## 2 RELATED WORKS

*3D Generation.* Early works in 3D shape generation utilized generative adversarial networks [Goodfellow et al. 2016] to synthesize 3D shapes from random noise [Chen and Zhang 2019; Wu et al. 2016; Zheng et al. 2022]. More recently, the focus has shifted toward adapting diffusion models [Ho et al. 2020] for 3D generation across various 3D representations, including voxels [Cheng et al. 2023; Chou et al. 2023; Hui et al. 2022; Li et al. 2023; Shim et al. 2023], point clouds [Luo and Hu 2021; Nichol et al. 2022; Zeng et al. 2022], triplanes [Gupta et al. 2023; Shue et al. 2023], implicit shape functions [Erkoç et al. 2023; Jun and Nichol 2023; Zhang et al. 2023, 2024b], Gaussian splattings [Roessle et al. 2024], and sparse voxel structures [Liu et al. 2023b; Ren et al. 2024; Xiang et al. 2024; Xiong et al. 2024a,b; Zheng et al. 2023]. While these methods have achieved remarkable results, their generation paradigms differ fundamentally from those of autoregressive models [OpenAI 2023; Touvron et al. 2023; Wang et al. 2024b]. In this paper, we explore the potential of autoregressive models for 3D shape generation, with the aim of laying a foundation for general multimodal models capable of simultaneously generating 3D shapes, images, and text.

*3D Autoregressive Models.* Inspired by the success of autoregressive models in text and image generation, several pioneering works have begun exploring their application to 3D shape generation. A few methods leverage autoregressive models to generate 3D meshes [Chen et al. 2024a,c; Hao et al. 2024; Nash et al. 2020; Siddiqui et al. 2024; Wang et al. 2024a; Weng et al. 2024], mainly by predicting vertices and faces in a predefined rasterization order. There are also works that autoregressively generate 3D shapes in point clouds [Cheng et al. 2022; Sun et al. 2020]. Following trends in image generation, an intuitive extension involves training a VQ-VAE [van den Oord et al. 2017] to compress 3D shapes into low-dimensional latent spaces [Cheng et al. 2022; Mittal et al. 2022; Qian et al. 2024; Yan et al. 2022; Zhang et al. 2022] before training autoregressive models to improve efficiency. However, these methods face challenges in capturing complex geometric details due to the long sequence lengths required to encode intricate textures and structures of 3D shapes. Additionally, their serialization methods often disregard the hierarchical structure and spatial locality inherent to 3D shapes, leading to slower training convergence. Autoregressive models have also been explored for scene layout generation [Paschalidou et al. 2021; Wang et al. 2021]. Concurrently, recent works have extended the next-scale prediction paradigm, initially introduced for image generation [Tian et al. 2024], to 3D shape generation by constructing multiscale latent spaces [Chen et al. 2024b; Zhang et al. 2024c,d]. Our work addresses limitations of previous works by proposing a novel autoregressive model that generates 3D shapes in a novel binarized octree representation and introduces efficient transformer architectures to capture long-range dependencies in token sequences.

The work most closely related to our OctGPT is the Octree Transformer proposed by [Ibing et al. 2023]. However, while Octree Transformers primarily focus on compressing octree sequence lengths for efficient training, our method introduces novel transformer architectures and generation schemes to enhance efficiency. Additionally, Octree Transformers predict the coordinates of octree nodes directly,

whereas our approach predicts the binary splitting status of octree nodes, significantly improving the quality of the generated shapes. Moreover, Octree Transformers are limited to generating sparse voxels, whereas our method produces continuous implicit fields, which can be converted into high-resolution meshes.

*3D Transformers.* Autoregressive models primarily rely on transformers [Vaswani et al. 2017] to learn dependencies within token sequences. Transformers have been adapted to 3D data by treating each point or patch as a token and applying attention mechanisms globally across all tokens [Guo et al. 2021; Pang et al. 2022; Yu et al. 2022]. However, these methods are limited to small-scale point clouds with only a few thousand tokens due to the huge computational and memory costs of global attention mechanisms. To address these issues, several works have proposed to constrain attention modules to operate within local neighborhoods [Wu et al. 2022; Zhao et al. 2021] or non-overlapping windows of point clouds [Fan et al. 2022; Lai et al. 2022; Sun et al. 2022; Yang et al. 2024]. More recently, the OctFormer [Wang 2023] and its variants [Wu et al. 2024] introduced a novel approach by serializing point tokens along z-order or Hilbert curves and partitioning the resulting token sequences into windows with equal token counts before applying attention mechanisms. This design achieves state-of-the-art performance on large-scale 3D understanding benchmarks. Our work builds on the principles of OctFormer, but we shift the focus from 3D understanding tasks to autoregressive 3D shape generation. Furthermore, we extend OctFormer to handle multiscale token sequences by incorporating scale-specific embeddings into the transformer architecture.

## 3 METHOD

Our goal is to harness autoregressive models for 3D shape generation. This involves two key components: a serialized representation of 3D shapes and an autoregressive model. The overview of our model is presented in Fig. 2. We first introduce a novel serialized octree representation, produced by an octree-based VQVAE [van den Oord et al. 2017], which encodes 3D shapes into multiscale binary token sequences. The details of this representation are elaborated in Section 3.1. Next, we train transformers to autoregressively predict these sequences, enabling the generation of 3D shapes from coarse to fine. To enhance efficiency and performance, we incorporate octree-based attention mechanisms [Wang 2023], multi-token prediction strategies [Li et al. 2024], and customized 3D positional encodings, achieving substantial improvements in training and generation performance, as described in Section 3.2.

### 3.1 Serialized Octree Representation

Our representation consists of two components: an octree and quantized binary codes produced by an octree-based VQVAE. The octree captures the coarse geometric structure of the shape, while the VQVAE encodes fine-grained details and is responsible for reconstructing the continuous signed distance fields (SDFs). Both the octree structure and the quantized codes are serialized into a binary sequence, serving as input to the subsequent autoregressive model.

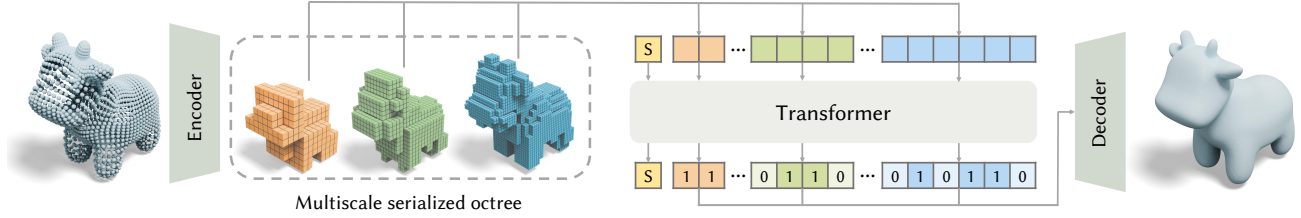


Fig. 2. Overview. 3D shapes are encoded as multiscale serialized octrees, where coarse structures are represented by multiscale binary splitting signals derived from the octree hierarchy, and fine-grained details are captured by binarized latent codes from an octree-based VQVAE. These binary tokens, along with teacher-forcing masks, are fed into a transformer for autoregressive training. During inference, the transformer progressively predicts the token sequence to reconstruct the octree and latent codes, generating 3D shapes from coarse to fine. The sequence is decoded by the VQVAE to produce the final 3D shape.

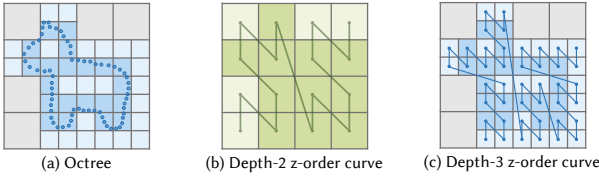


Fig. 3. Octree and z-order curves. 2D images are used for clearer illustration. (a): The input point cloud with its corresponding octree. Node statuses are color-coded: darker colors represent nodes containing points, lighter colors indicate empty nodes, and gray denotes non-existing nodes at the given depth. (b) & (c): z-order curves at octree depths 2 and 3, respectively.

**3.1.1 Serialized Octree.** Given a 3D shape, we first rescale it to fit within a unit cube and construct an octree by recursively subdividing non-empty voxels until a specified depth is reached [Wang 2023; Zhou et al. 2011]. Additionally, we enforce the first three levels of the octree to be fully populated, which covers the entire volume, including any disconnected components. The octree structure is determined by the split status at each node, with nodes sorted in z-order according to shuffled keys [Zhou et al. 2011]. Notably, spatial locality is well preserved in the octree due to the z-order, *i.e.*, octree nodes that are spatially close are likely to be adjacent in the z-order curve. An example is shown in Fig. 3.

Denote the maximum depth of the octree as  $D$ , and the node split status at depth  $d$  as  $o_i^d \in \{0, 1\}$ , where  $i$  is the node index in the z-order curve and 0/1 indicate no split/split, respectively. The octree nodes at depth  $d$  are concatenated into a binary sequence  $O^d = (o_1^d, o_2^d, \dots, o_{n_d}^d)$ , where  $n_d$  is the number of nodes at depth  $d$ . At depth 3, the octree is fully populated, resulting in 512 nodes. Starting from depth 3, the binary sequences from each level up to depth  $(D - 1)$  are concatenated, forming a multiscale binary sequence  $O = (O^3, O^4, \dots, O^{D-1})$ . Inversely, this sequence  $O$  can be used to reconstruct the octree structure, effectively capturing the coarse geometry of a 3D shape.

**3.1.2 Octree-based VQVAE.** Complementing the octree, we introduce an octree-based VQVAE for efficient tokenization and reconstruction of SDFs and geometric details of 3D shapes. The VQVAE generates *quantized binary codes* at the finest level of the octree. The detailed architecture of the VQVAE is illustrated in Fig. 4. Our

VQVAE model employs an asymmetric encoder-decoder architecture, with a particular emphasis on enhancing the decoder’s ability to achieve high-fidelity surface reconstruction.

The encoder is based on octree-based CNNs (O-CNN) [Wang et al. 2017]. Starting with an octree constructed from a 3D mesh or point cloud, the encoder efficiently compresses the input octree into feature representations at the leaf nodes, reducing the depth of the octree by 2. These features are then quantized into binary tokens using the Binary Spherical Quantization (BSQ) method [Zhao et al. 2024]. Specifically, the feature vector  $z_i \in \mathbb{R}^d$  at the  $i^{\text{th}}$  leaf node is quantized into binary tokens  $q_i$  as follows:  $q_i = \text{sign}\left(\frac{z_i}{\|z_i\|}\right)$ . The BSQ eliminates the need for codebooks, as required in conventional VQ-VAEs, thereby simplifying implementation while maintaining comparable reconstruction quality. Following [Zhao et al. 2024], we also employ a loss function, denoted as  $\mathcal{L}_{oq}$ , to encourage the binary tokens to be uniformly distributed.

Subsequently, the decoder employs the dual octree graph networks [Wang et al. 2022] to decode the binary tokens  $q_i$  into local SDFs, which are then integrated into a global SDF using the multi-level Partition-of-Unity method [Ohtake et al. 2003; Wang et al. 2022]. This process ensures a coherent and detailed reconstruction of the original shape. The loss for SDF reconstruction is defined as:

$$\mathcal{L}_{sdf} = \frac{1}{N_{\mathcal{P}}} \sum_{x \in \mathcal{P}} \left( \lambda \|S(x) - D(x)\|_2^2 + \|\nabla S(x) - \nabla D(x)\|_2^2 \right), \quad (1)$$

where  $S(x)$  and  $D(x)$  are the predicted and ground-truth SDFs, respectively,  $\lambda$  is a weighting factor,  $\mathcal{P}$  is the set of sampled points, and  $N_{\mathcal{P}}$  is the number of sampled points. This loss encourages the decoder to reconstruct the continuous SDFs accurately. Since the encoder reduces the depth of the octree, the decoder is designed to recover the original octree depth with an octree splitting loss  $\mathcal{L}_{octree}$ , following [Wang et al. 2022, 2018].

In total, the loss of the VQVAE is defined as:

$$\mathcal{L} = \mathcal{L}_{oq} + \mathcal{L}_{sdf} + \mathcal{L}_{octree}. \quad (2)$$

The binary tokens  $q_i$  produced by the encoder are also serialized according to the z-order curve, forming the sequence  $Q$ , which is concatenated with  $O$  to create our final serialized octree representation.

*Remarks.* Our serialized octree representation consists entirely of binary tokens, which can be easily processed and predicted by autoregressive models. Furthermore, our representation captures multiscale information of the 3D shape and preserves the spatial

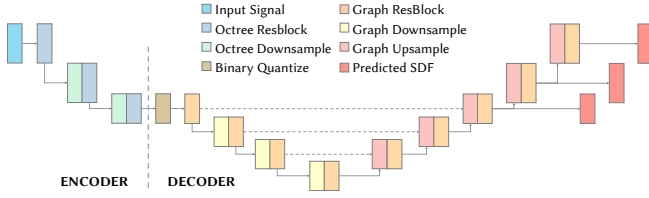


Fig. 4. The architecture of Octree-based VQ-VAE. The encoder compresses the input octree signals with octree-based residual blocks and reduce the depth of the octree by 2. The features are then quantized into binary tokens and fed into the decoder. The decoder builds a dual octree graph and applies graph convolution to predict SDFs for shape reconstruction.

locality of octree nodes. These properties make it more suitable for autoregressive prediction compared to the commonly used rasterization order in previous works [Siddiqui et al. 2024; Yan et al. 2022; Zhang et al. 2022], as examined in our experiments in Section 4.2.

### 3.2 Multiscale Autoregressive Models

Using our serialized octree representation, we can train autoregressive models to predict it, enabling the progressive generation of 3D shapes from coarse to fine. While directly applying standard autoregressive models [Brown et al. 2020; Touvron et al. 2023] to this representation is feasible, it is computationally inefficient and often results in suboptimal performance. To overcome these challenges, we introduce three key enhancements, including an efficient transformer architecture, customized positional encoding, and multi-token generation strategies, significantly improving the training and generation efficiency.

**3.2.1 Efficient Transformer Architecture.** Our transformer architecture consists of a stack of attention blocks [Vaswani et al. 2017], each containing a multi-head self-attention module and a feed-forward network with layer normalization and residual connections. Given that token sequences can exceed  $50k$  in length, computing self-attention over all tokens is computationally prohibitive. To address this, we adopt octree-based attentions (OctFormer) [Wang 2023], which divide tokens into fixed-size windows for efficient self-attention computation. Furthermore, we alternate between *dilated* octree attention and *shifted* window attention [Yang et al. 2024], enabling interactions across different windows. The illustration of octree-based attention and shifted window attention is shown in Fig. 5-(b)&(c). Unlike OctFormer, which restricts tokens to a single octree depth, our design accommodates tokens from nodes at varying depths, allowing comprehensive interactions among all tokens. This approach captures both local and global dependencies, enhancing the model’s ability to represent 3D shapes.

**3.2.2 Positional Encoding.** As transformers are permutationally invariant, positional information must be incorporated into the model. Each token in the sequence corresponds to an octree node with a 3D position within the unit cube and an associated depth. To encode positional information, we propose RoPE3D that extends rotary positional encoding (RoPE) [Su et al. 2024] to 3D space, inspired by the RoPE2D design [Heo et al. 2025]. Additionally, we

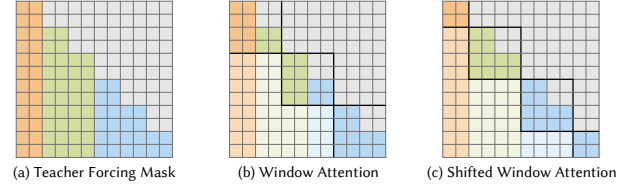


Fig. 5. Multiscale Autoregressive Models. (a) Our model predicts multiple tokens autoregressively according to the depth-wise teacher-forcing mask. Tokens at different scales are represented in distinct colors, while masks are depicted in gray. (b) Octree-based Window attention is adopted for cross-scale communication and improved computational efficiency. (c) Shifted window attention allows for interactions across different windows.

introduce learnable scale embeddings to differentiate tokens at different octree depths. By integrating 3D positional encoding with scale embeddings, our transformer can effectively distinguish tokens based on their spatial positions and depths, which is crucial for accurate autoregressive prediction of 3D shapes. The effectiveness of our positional encoding is demonstrated through experiments presented in Section 4.2.

**3.2.3 Multiple Token Generation.** Standard autoregressive models predict one token at a time, which can be inefficient for generating 3D shapes due to the large number of tokens involved. To address this limitation, we adopt the multi-token generation strategy proposed in masked autoregressive models (MAR) [Li et al. 2024], which enables the parallel prediction of multiple tokens. This approach significantly reduces the number of forward passes required for 3D shape generation, thereby improving efficiency.

MAR operates by randomly permuting tokens in the sequence and masking a portion of them, which are then predicted by the model in an autoregressive manner. However, directly applying MAR to our sequence can lead to dependency issues since our sequence comprises tokens from multiple octree depths, where tokens at deeper octree layers depend on those from shallower layers. To address this challenge, we introduce a depth-wise teacher-forcing mask, as illustrated in Fig. 5-(a). Instead of permuting the whole sequence, we permute tokens within each depth level, ensuring that tokens at higher depths can access information from lower-depth tokens while preventing information leakage from higher-depth tokens. By doing so, it preserves the hierarchical dependencies in the sequence.

During inference, token prediction begins at depth 3 and proceeds sequentially to the maximum octree depth  $D$ . Tokens from depths 3 to  $(D - 1)$  are interpreted as split signals, progressively generating coarse voxel grids and refining them into deeper octrees. Tokens at depth  $D$  are decoded as binary quantized codes, capturing the fine details of the 3D shape. Both split signals and quantized codes are binary tokens and are predicted using binary classifiers attached on the transformer. The predicted sequence is then fed into the VQVAE decoder to reconstruct the final 3D shape.

## 4 EXPERIMENTS

In this section, we evaluate the performance and efficiency of our OctGPT on 3D shape generation tasks in Section 4.1, conduct ablation studies in Section 4.2, and demonstrate the versatility of our

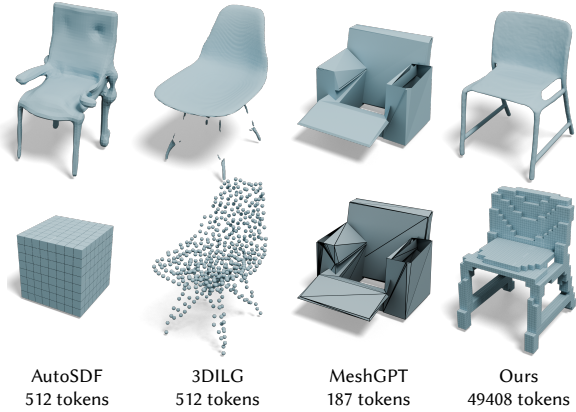


Fig. 6. Comparison with state-of-the-art 3D autoregressive models. Experiments are conducted on the chair category. Top: the generated shapes. Bottom: the corresponding token.

model through various applications in Section 4.3. All experiments are performed using *NVIDIA 4090 GPUs* with 24GB of memory.

#### 4.1 3D Shape Generation

In this section, we evaluate the performance of our model and compare it with state-of-the-art methods on the ShapeNet [Chang et al. 2015] and Objaverse [Deitke et al. 2023] datasets. The datasets and implementation details are provided in the supplementary material.

*Comparisons.* We conduct comparisons with state-of-the-art 3D generation methods, including IM-GAN [Chen and Zhang 2019], SDF-StyleGAN [Zheng et al. 2022], Wavelet-Diffusion [Hui et al. 2022], MeshDiffusion [Liu et al. 2023a], SPAGHETTI [Hertz et al. 2022], LAS-Diffusion [Zheng et al. 2023], 3DILG [Zhang et al. 2022], and 3DShape2VecSet [Zhang et al. 2023]. Among them, IM-GAN and SDF-StyleGAN are GAN-based methods, Wavelet-Diffusion, MeshDiffusion, SPAGHETTI, and LAS-Diffusion are diffusion-based methods, while AutoSDF, 3DILG, and MeshGPT are autoregressive methods, which are most closely related to our approach. We did not include comparisons with MeshAnything [Chen et al. 2024a], MeshAnything-v2 [Chen et al. 2024c], or Edgerunner [Tang et al. 2024b], as these methods mainly focus on artistic mesh generation conditioned on point clouds, dense meshes, or images.

The quantitative FID results are presented in Table 1. Note that Wavelet-Diffusion was trained on only three categories, SPAGHETTI and MeshGPT were trained on two categories only, and the training datasets for MeshGPT, 3DILG and 3DShape2VecSet differ slightly from those of the other methods. The upper part of the table shows the results for training on each category separately, while the lower part presents the results for training on all categories together. We perform category-conditional generation when trained on all categories together. Our OctGPT consistently outperforms other methods across most categories, even surpassing state-of-the-art diffusion-based methods like OctFusion and XCube in the *Car* and *Rifle* categories. Qualitative results are shown in Fig. 8, where our method generates more detailed shapes than the competing approaches. Note that diffusion-based methods [Ren et al. 2024; Zheng

Table 1. The quantitative comparison of *shading-image-based FID*. The upper part shows results for training on each category separately, while the lower part shows results for training on all categories together. Shaded rows indicate autoregressive models, and green numbers highlight the improvement of our OctGPT in FID score over the previous best-performing autoregressive models. On average, OctGPT achieves the best performance.

Method	Chair	Airplane	Car	Table	Rifle
IM-GAN	63.42	74.57	141.2	51.70	103.3
SDF-StyleGAN	36.48	65.77	97.99	39.03	64.86
Wavelet-Diffusion	28.64	35.05	N/A	30.27	N/A
MeshDiffusion	49.01	97.81	156.21	49.71	87.96
SPAGHETTI	65.26	59.21	N/A	N/A	N/A
LAS-Diffusion	20.45	32.71	80.55	17.25	44.93
XCube	18.07	<b>19.08</b>	80.00	N/A	N/A
OctFusion	<b>16.15</b>	24.29	78.00	<b>17.19</b>	30.56
MeshGPT	37.05	N/A	N/A	25.25	N/A
OctGPT	31.05 <span style="color: green;">↓6.00</span>	27.47	<b>64.45</b>	19.64 <span style="color: green;">↓5.61</span>	<b>21.91</b>
3DShape2VecSet	21.21	46.27	110.12	25.15	54.20
LAS-Diffusion	21.55	43.08	86.34	<b>17.41</b>	70.39
OctFusion	<b>19.63</b>	30.92	80.97	17.49	28.59
3DILG	31.64	54.38	164.15	54.13	77.74
OctGPT	28.28 <span style="color: green;">↓3.36</span>	<b>29.27</b> <span style="color: green;">↓25.11</span>	<b>62.40</b> <span style="color: green;">↓101.75</span>	20.64 <span style="color: green;">↓33.49</span>	<b>27.21</b> <span style="color: green;">↓50.53</span>

et al. 2023] often require multiple cascaded stages or auxiliary models, resulting in increased implementation complexity and potential error accumulation. Moreover, diffusion models fundamentally differ from autoregressive frameworks in their generative mechanisms, which may limit their ability to achieve seamless multimodal integration.

Compared to previous autoregressive methods such as AutoSDF, 3DILG and MeshGPT, OctGPT achieves a significant improvement in FID performance. Specifically, OctGPT achieves an average improvement of 42.84 in FID score over 3DILG, which is the previous best-performing autoregressive model for 3D shape generation. We visualize the token sequences of these autoregressive methods in Fig. 6. OctGPT is capable of processing significantly longer sequences, allowing it to capture finer details and generate higher-quality shapes. For efficiency, OctGPT achieves a 34× speedup over 3DILG at a sequence length of 80K, while AutoSDF and MeshGPT run out of memory at this sequence length, demonstrating OctGPT’s superior memory and computational efficiency. Moreover, OctGPT uses fewer parameters, requires fewer training epochs, and consumes less GPU memory, highlighting its faster convergence and significantly reduced computational demands. Detailed comparisons are provided in the supplementary material.

*More Generation Results.* We also train our model on 13 categories from the ShapeNet and the Objaverse dataset to demonstrate its scalability to a larger number of categories. The results are presented in Fig. 7. Our model generates high-quality and diverse shapes across different categories. The generated shapes exhibit rich details, and the overall quality remains consistent with the results obtained from the five categories of ShapeNet.





Fig. 12. Comparison with 3D causal autoregressive model. Experiments are conducted on the airplane category.

## 4.2 Ablation Study and Discussions

In this section, we conduct ablation studies to analyze the impact of key design choices in our model. We conduct experiments on the airplane category from ShapeNet.

*Multiscale Autoregressive Models.* One of our key design innovations is training autoregressive models on serialized multiscale binary tokens induced by octrees. These multiscale binary tokens effectively decompose the challenging task of modeling 3D positions into a series of simpler binary classification tasks, which significantly enhances both training efficiency and the modeling capacity of autoregressive models. We compare our model with a baseline autoregressive model trained on single-scale 3D positions. Apart from the multiscale binary tokens, octrees can also be fully determined by their finest nodes, which are described by sparse 3D positions. We sort these 3D positions in rasterized order, as done in 3DILG [Zhang et al. 2022] and MeshGPT [Siddiqui et al. 2024], and train autoregressive models on these positions. To highlight the effectiveness of our multiscale binary tokens, we maintain identical model architecture and training settings for a fair comparison. The training results are shown in Fig. 12. With our multiscale binary tokens, our model achieves a significant improvement in FID score from 142.92 to 27.47 and generation quality. Furthermore, the convergence speed is much faster: after just 10 epochs, our model outperforms the baseline model, which was trained for 100 epochs.

*Efficiency.* The second key design innovation is extending octree-based window attention to our multiscale binary sequence and introducing multiple token prediction for efficient training and generation. We analyze the impact of these designs on the efficiency of our model using a single NVIDIA 4090 GPU. The results are shown in Fig. 13. It can be seen that we speed up training by 13 $\times$  when the token length exceeds 160k compared to standard global attention, and we improve generation speed by over 69 $\times$  when the token length exceeds 40k compared to single-token prediction. These designs bring significant efficiency improvements to our model, making our experiments feasible on 4 NVIDIA 4090 GPUs, which allows our model to be easily scaled up and makes it more accessible to a wider range of researchers.

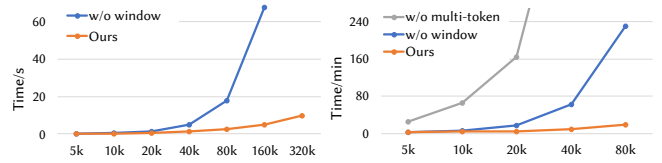


Fig. 13. Ablation study on efficiency. The time consumption in training and generation are shown in the left and right plots, respectively. The X-axis represents the token length. The training time is measured per iteration, and the generation time is measured per mesh.

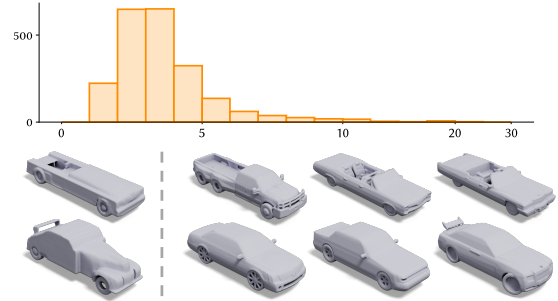


Fig. 14. Diversity. Top: Histogram of Chamfer Distance (CD) between generated shapes and the training set. Bottom: The generated meshes (left) and the 3 nearest shapes (right) from the training dataset according to CD.

*Position Encoding.* The proposed RoPE3D and learnable depth embeddings are crucial for our model to capture the spatial and scale relationships among tokens. We conduct experiments to assess the impact of these components by removing them sequentially. The results are shown in Table 2.

*Z-order.* Previous 3D autoregressive models rely on rasterization-ordered positions [Siddiqui et al. 2024; Zhang et al. 2022], whereas we adopt the z-ordering induced by octrees. By preserving spatial locality, z-ordering allows the transformer to more effectively model highly correlated tokens. We validate the advantages of z-ordering through ablation studies, as shown in Table 2.

*Tradeoff between Quality and Speed.* Our model supports parallel token generation, enabling a flexible tradeoff between generation speed and the quality of the generated shapes. Specifically, we can generate more tokens in parallel to accelerate the generation process, while sacrificing some quality. In the extreme case, we can generate one token at a time, which corresponds to the standard autoregressive generation approach. To analyze this tradeoff, we conduct experiments to evaluate the relationship between the number of tokens generated in parallel and the generation speed. The results are shown in Table 2.

*Diversity.* We follow the protocol from LAS-Diffusion [Zheng et al. 2023] and Wavelet-Diffusion [Hui et al. 2022] to assess the diversity of the generated shapes of our OctGPT. Specifically, we compute the Chamfer distance between the generated shapes and the training set, and construct a histogram with the x-axis representing the Chamfer distance, as shown in Fig. 14. The results demonstrate that our model

Table 2. Ablation studies on positional encodings and z-order (left) and number of generation iterations (right). The FID values are reported for the airplane category. Time indicates the time consumption to generate a mesh.

Method	FID	$N_{iter}$	FID	Time
w/o RoPE3D	38.03	64	35.95	6.43s
w/o Scale Embeddings	34.41	128	33.60	9.65s
w/o z-order	43.71	256	31.90	17.05s
Ours	27.47	512	27.47	34.51s

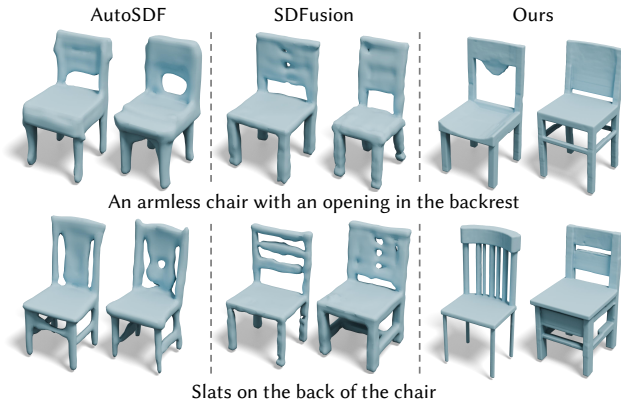


Fig. 15. Comparison of text conditional generation results. Experiments are conducted on the chair category of ShapeNet dataset.

is capable of generating novel shapes with high diversity, as the majority of the generated shapes differ from those in the training set. In the bottom row of Fig. 14, we display some generated samples alongside the three most similar shapes retrieved from the training set.

### 4.3 Applications

**Text-Conditioned Generation.** Given text prompts, we leverage text encoder of CLIP [Radford et al. 2021] to extract text features and integrate the extracted features into the generation process through cross-attention modules [Vaswani et al. 2017]. We compare our method with AutoSDF [Mittal et al. 2022] and SDFusion [Cheng et al. 2023] on Text2Shape dataset [Chen et al. 2018], as shown in Fig. 15. We also compare with Shap-E [Jun and Nichol 2023], Gaussian Cube [Zhang et al. 2024a] and LN3Diff [Lan et al. 2024] on Objaverse dataset, as shown in Fig. 10. It can be observed that other methods produce shapes that suffer from distortions and artifacts, whereas our method generates shapes with superior quality and greater diversity.

**Sketch-Conditioned Generation.** We conduct sketch-conditioned generation to demonstrate the generalization ability and versatility of our OctGPT. The sketch data are created following LAS-Diffusion [Zheng et al. 2023], and we train our model on the airplane and car categories for 100 epochs. The sketch input is encoded by a pre-trained Dinov2 [Oquab et al. 2023] and then integrated into the OctGPT model. Notably, our model does not rely on view information; instead, we replace the view-aware attention mechanism in LAS-Diffusion with standard cross-attention modules. Despite this,

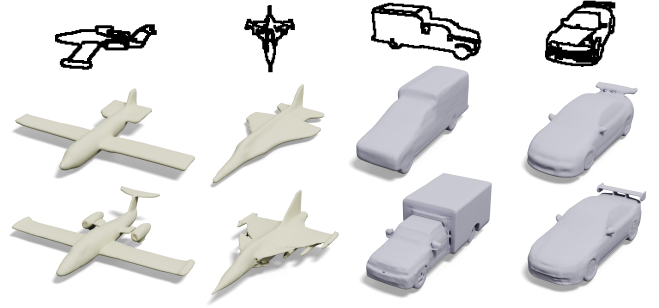


Fig. 16. Comparison of sketch conditional generation results. Experiments are conducted on the airplane and car category of ShapeNet dataset. Top: input sketches. Middle row: shapes generated by LAS-Diffusion. Bottom: shapes generated by our OctGPT.



Fig. 17. Qualitative results of image conditioned generation. Experiments are conducted on the airplane and car category of ShapeNet dataset.

our model is still able to generate high-quality shapes that are consistent with the input sketches, as shown in Fig. 16. The geometric details are more realistic compared to the results from LAS-Diffusion.

**Image-conditioned Generation.** The sketch-conditioned generation can be easily extended to image-conditioned generation. Specifically, we utilized rendered images from ShapeNet [Chang et al. 2015] during training. The training settings are the same as those used for sketch-conditioned generation. The qualitative results are shown in Fig. 17. It can be observed that our method generates shapes that are consistent with the input images and preserve their details.

**Scene-level Generation.** We also perform a challenging stress test on our OctGPT by generating scenes with multiple objects. We use the synthetic room dataset [Peng et al. 2020], which contains 5k scenes, each composed by randomly selecting objects from five categories of ShapeNet: chair, sofa, lamp, cabinet, and table. We train our model on this dataset and generate scenes at a resolution of  $1024^3$ . The model is trained for 200 epochs on 4 NVIDIA 4090 GPUs, taking approximately 3 days. Surprisingly, our model generates diverse scenes with multiple objects, as shown in Fig. 11. The generated scenes are visually appealing and exhibit rich details, demonstrating the scalability and versatility of our model. In comparison, training a standard autoregressive model on the serialized 3D positions results in poor performance, with the model struggling to generate meaningful results due to the complexity of scene-level generation.

## 5 CONCLUSIONS

In this paper, we presented *OctGPT*, a novel approach for efficient and high-quality 3D shape generation using a multiscale autoregressive model based on serialized octree representations. The core idea behind OctGPT is to encode 3D shapes as multiscale binary sequences induced by octrees, and then use an autoregressive transformer model for 3D shape generation. We also introduced an efficient transformer architecture that incorporates extended octree attention mechanisms, tailored 3D rotary positional encodings, and parallelized token generation schemes. OctGPT significantly advances the state-of-the-art in 3D shape generation with autoregressive models, and scalability, and even surpassing existing diffusion models in some cases. We demonstrated the scalability and versatility of OctGPT across a wide range of 3D shape generation tasks.

There are a few limitations and exciting future directions. Firstly, our model is a two-stage pipeline: generating serialized octree representations via VQVAE, followed by 3D shape generation using an autoregressive transformer. While effective, this approach is not end-to-end trainable, which may constrain the model's overall performance. Future work can focus on developing end-to-end training strategies. Secondly, our model has been trained with limited GPU resources. We plan to leverage additional computational resources and larger datasets to further enhance scalability and performance. Lastly, exploring multi-modality training is an exciting direction that could broaden OctGPT's applicability by enabling it to handle diverse input modalities, which would open up new possibilities for integrating 3D shape generation with other modalities.

## ACKNOWLEDGMENTS

This work was supported in part by National Key R&D Program of China 2022ZD0160801 and Beijing Natural Science Foundation No. 4244081. We also thank the anonymous reviewers for their invaluable feedback.

## REFERENCES

- Tom Brown, Benjamin Mann, Nick Ryder, Melanie Subbiah, Jared D Kaplan, Prafulla Dhariwal, Arvind Neelakantan, Pranav Shyam, Girish Sastry, Amanda Askell, et al. 2020. Language models are few-shot learners. In *NeurIPS*.
- Angel X. Chang, Thomas Funkhouser, Leonidas J. Guibas, Pat Hanrahan, Qixing Huang, Zimo Li, Silvio Savarese, Manolis Savva, Shuran Song, Hao Su, Jianxiong Xiao, Li Yi, and Fisher Yu. 2015. ShapeNet: An information-rich 3D model repository. *arXiv preprint arXiv:1512.03012* (2015).
- Kevin Chen, Christopher B. Choy, Manolis Savva, Angel X Chang, Thomas Funkhouser, and Silvio Savarese. 2018. Text2Shape: Generating Shapes from Natural Language by Learning Joint Embeddings. *arXiv preprint arXiv:1803.08495* (2018).
- Yiwen Chen, Tong He, Di Huang, Weicai Ye, Sijin Chen, Jiayang Tang, Xin Chen, Zhongang Cai, Lei Yang, Gang Yu, et al. 2024a. MeshAnything: Artist-Created Mesh Generation with Autoregressive Transformers. *arXiv preprint arXiv:2406.10163* (2024).
- Yongwei Chen, Yushi Lan, Shangchen Zhou, Tengfei Wang, and Xingang Pan. 2024b. SAR3D: Autoregressive 3D object generation and understanding via multi-scale 3D VQVAE. *arXiv preprint arXiv:2411.16856* (2024).
- Yiwen Chen, Yikai Wang, Yihao Luo, Zhengyi Wang, Zilong Chen, Jun Zhu, Chi Zhang, and Guosheng Lin. 2024c. Meshanything v2: Artist-created mesh generation with adjacent mesh tokenization. *arXiv preprint arXiv:2408.02555* (2024).
- Zhiqin Chen and Hao Zhang. 2019. Learning implicit fields for generative shape modeling. In *CVPR*.
- An-Chieh Cheng, Xueting Li, Sifei Liu, Min Sun, and Ming-Hsuan Yang. 2022. Autoregressive 3D shape generation via canonical mapping. In *ECCV*.
- Yen-Chi Cheng, Hsin-Ying Lee, Sergey Tuyakov, Alex Schwing, and Liangyan Gui. 2023. SDFusion: Multimodal 3D Shape Completion, Reconstruction, and Generation. In *CVPR*.
- Gene Chou, Yuval Bahat, and Felix Heide. 2023. Diffusion-SDF: Conditional Generative Modeling of Signed Distance Functions. In *ICCV*.
- Matt Deitke, Dustin Schwenk, Jordi Salvador, Luca Weihs, Oscar Michel, Eli Vander-Bilt, Ludwig Schmidt, Kiana Ehsani, Aniruddha Kembhavi, and Ali Farhadi. 2023. Objaverse: A universe of annotated 3D objects. In *CVPR*.
- Ziya Erkoç, Fangchang Ma, Qi Shan, Matthias Nießner, and Angela Dai. 2023. HyperDiffusion: Generating Implicit Neural Fields with Weight-Space Diffusion. In *ICCV*.
- Lue Fan, Ziqi Pang, Tianyuan Zhang, Yu-Xiong Wang, Hang Zhao, Feng Wang, Naiyan Wang, and Zhaoxiang Zhang. 2022. Embracing single stride 3D object detector with sparse transformer. In *CVPR*.
- Ian Goodfellow, Jean Pouget-Abadie, Mehdi Mirza, Bing Xu, David Warde-Farley, Sherjil Ozair, Aaron Courville, and Yoshua Bengio. 2016. Generative adversarial networks. In *NeurIPS*.
- Meng-Hao Guo, Jun-Xiong Cai, Zheng-Ning Liu, Tai-Jiang Mu, Ralph R Martin, and Shi-Min Hu. 2021. PCT: Point cloud transformer. *Comput. Vis. Media* 7, 2 (2021).
- Anchit Gupta, Wenhan Xiong, Yixin Nie, Ian Jones, and Barlas Ögüz. 2023. 3DGen: Triplane latent diffusion for textured mesh generation. *arXiv preprint arXiv:2303.05371* (2023).
- Zekun Hao, David W Romero, Tsung-Yi Lin, and Ming-Yu Liu. 2024. Meshtron: High-Fidelity, Artist-Like 3D Mesh Generation at Scale. *arXiv preprint arXiv:2412.09548* (2024).
- Byeongho Heo, Song Park, Dongyoon Han, and Sangdoon Yun. 2025. Rotary position embedding for vision transformer. In *ECCV*.
- Amir Hertz, Or Perel, Raja Giryes, Olga Sorkine-Hornung, and Daniel Cohen-Or. 2022. SPAGHETTI: Editing Implicit Shapes Through Part Aware Generation. *ACM Trans. Graph. (SIGGRAPH)* 41, 4 (2022).
- Jonathan Ho, Ajay Jain, and Pieter Abbeel. 2020. Denoising diffusion probabilistic models. In *NeurIPS*.
- Ka-Hei Hui, Ruihui Li, Jingyu Hu, and Chi-Wing Fu. 2022. Neural Wavelet-Domain Diffusion for 3D Shape Generation. In *SIGGRAPH Asia*.
- Moritz Ibing, Gregor Kobsik, and Leif Kobbelt. 2023. Octree Transformer: Autoregressive 3D Shape Generation on Hierarchically Structured Sequences. In *CVPR Workshops*.
- Heewoo Jun and Alex Nichol. 2023. Shap-E: Generating conditional 3D implicit functions. *arXiv preprint arXiv:2305.02463* (2023).
- Xin Lai, Jianhui Liu, Li Jiang, Liwei Wang, Hengshuang Zhao, Shu Liu, Xiaojuan Qi, and Jiaya Jia. 2022. Stratified Transformer for 3D Point Cloud Segmentation. In *CVPR*.
- Yushi Lan, Fangzhou Hong, Shuai Yang, Shangchen Zhou, Xuyi Meng, Bo Dai, Xingang Pan, and Chen Change Loy. 2024. LN3Diff: Scalable Latent Neural Fields Diffusion for Speedy 3D Generation. In *ECCV*.
- Muheng Li, Yueqi Duan, Jie Zhou, and Jiwen Lu. 2023. Diffusion-SDF: Text-to-Shape via Voxelized Diffusion. In *CVPR*.
- Tianhong Li, Yonglong Tian, He Li, Mingyang Deng, and Kaiming He. 2024. Autoregressive Image Generation without Vector Quantization. In *NeurIPS*.
- Hao Tian Liu, Chunyuan Li, Qingyang Wu, and Yong Jae Lee. 2024. Visual instruction tuning. In *NeurIPS*.
- Minghua Liu, Ruoxi Shi, Linghao Chen, Zhuoyang Zhang, Chao Xu, Xinyue Wei, Hansheng Chen, Chong Zeng, Jiayuan Gu, and Hao Su. 2023b. One-2-3-45+ : Fast single image to 3D objects with consistent multi-view generation and 3D diffusion. *arXiv preprint arXiv:2311.07885* (2023).
- Zhen Liu, Yao Feng, Michael J. Black, Derek Nowrouzezahrai, Liam Paull, and Weiyang Liu. 2023a. MeshDiffusion: Score-based Generative 3D Mesh Modeling. In *ICLR*.
- William E. Lorenson and Harvey E. Cline. 1987. Marching Cubes: A High Resolution 3D Surface Construction Algorithm. In *SIGGRAPH*.
- Ilya Loshchilov and Frank Hutter. 2019. Decoupled weight decay regularization. In *ICLR*.
- Shitong Luo and Wei Hu. 2021. Diffusion Probabilistic Models for 3D Point Cloud Generation. In *CVPR*.
- Tiang Luo, Chris Rockwell, Honglak Lee, and Justin Johnson. 2023. Scalable 3D Captioning with Pretrained Models. *arXiv preprint arXiv:2306.07279* (2023).
- Paritosh Mittal, Yen-Chi Cheng, Maneesh Singh, and Shubham Tulsiani. 2022. AutoSDF: Shape Priors for 3D Completion, Reconstruction and Generation. In *CVPR*.
- Charlie Nash, Yaroslav Ganin, SM Ali Eslami, and Peter Battaglia. 2020. PolyGen: An autoregressive generative model of 3D meshes. In *ICML*.
- Alex Nichol, Heewoo Jun, Prafulla Dhariwal, Pamela Mishkin, and Mark Chen. 2022. Point-E: A system for generating 3D point clouds from complex prompts. *arXiv preprint arXiv:2212.08751* (2022).
- Yutaka Ohtake, Alexander Belyaev, Marc Alexa, Greg Turk, and Hans-Peter Seidel. 2003. Multi-level partition of unity implicits. *ACM Trans. Graph. (SIGGRAPH)* 22, 3 (2003).
- OpenAI. 2023. GPT-4 Technical Report. *arXiv preprint arXiv:2303.08774* (2023).
- Maxime Oquab, Timothée Darcet, Théo Moutakanni, Huy Vo, Marc Szafraniec, Vasil Khalidov, Pierre Fernandez, Daniel Haziza, Francisco Massa, Alaaeldin El-Nouby, et al. 2023. DINOv2: Learning robust visual features without supervision. *arXiv preprint arXiv:2304.07193* (2023).

- Long Ouyang, Jeffrey Wu, Xu Jiang, Diogo Almeida, Carroll Wainwright, Pamela Mishkin, Chong Zhang, Sandhini Agarwal, Katarina Slama, Alex Ray, et al. 2022. Training language models to follow instructions with human feedback. In *NeurIPS*.
- Yatian Pang, Wenxiao Wang, Francis EH Tay, Wei Liu, Yonghong Tian, and Li Yuan. 2022. Masked autoencoders for point cloud self-supervised learning. In *ECCV*.
- Despoina Paschalidou, Amlan Kar, Maria Shugrina, Karsten Kreis, Andreas Geiger, and Sanja Fidler. 2021. Atiss: Autoregressive transformers for indoor scene synthesis. In *NeurIPS*.
- Songyu Peng, Michael Niemeyer, Lars Mescheder, Marc Pollefeys, and Andreas Geiger. 2020. Convolutional occupancy networks. In *ECCV*.
- Xuelin Qian, Yu Wang, Simian Luo, Yinda Zhang, Ying Tai, Zhenyu Zhang, Chengjie Wang, Xiangyang Xue, Bo Zhao, Tiejun Huang, Yunsheng Wu, and Yanwei Fu. 2024. Pushing Auto-regressive Models for 3D Shape Generation at Capacity and Scalability. *arXiv preprint arXiv:2402.12225* (2024).
- Alec Radford, Jong Wook Kim, Chris Hallacy, Aditya Ramesh, Gabriel Goh, Sandhini Agarwal, Girish Sastry, Amanda Askell, Pamela Mishkin, Jack Clark, et al. 2021. Learning transferable visual models from natural language supervision. In *ICML*.
- Xuanchi Ren, Jiahui Huang, Xiaohui Zeng, Ken Museth, Sanja Fidler, and Francis Williams. 2024. XCube ( $X^3$ ): Large-Scale 3D Generative Modeling using Sparse Voxel Hierarchies. In *CVPR*.
- Barbara Roessle, Norman Müller, Lorenzo Porzi, Samuel Rota Bulò, Peter Kotschieder, Angela Dai, and Matthias Nießner. 2024. L3DG: Latent 3D Gaussian Diffusion. In *SIGGRAPH Asia*.
- Jaehyeok Shim, Changwoo Kang, and Kyungdon Joo. 2023. Diffusion-based Signed Distance Fields for 3D Shape Generation. In *CVPR*.
- J. Ryan Shue, Eric Ryan Chan, Ryan Po, Zachary Anknor, Jiajun Wu, and Gordon Wetzstein. 2023. 3D Neural Field Generation using Triplane Diffusion. In *CVPR*.
- Yavar Siddiqui, Antonio Alliegro, Alexey Artemov, Tatiana Tommasi, Daniele Sirigatti, Vladislav Rosov, Angela Dai, and Matthias Nießner. 2024. MeshGPT: Generating triangle meshes with decoder-only transformers. In *CVPR*.
- Jianlin Su, Murtadha Ahmed, Yu Lu, Shengfeng Pan, Wen Bo, and Yunfeng Liu. 2024. RoFormer: Enhanced transformer with rotary position embedding. *Neurocomputing* (2024).
- Peize Sun, Yi Jiang, Shoufa Chen, Shilong Zhang, Bingyue Peng, Ping Luo, and Zehuan Yuan. 2024. Autoregressive Model Beats Diffusion: Llama for Scalable Image Generation. *arXiv preprint arXiv:2406.06525* (2024).
- Pei Sun, Mingxing Tan, Weiye Wang, Chenxi Liu, Fei Xia, Zhaoqi Leng, and Dragomir Anguelov. 2022. SWFormer: Sparse Window Transformer for 3D Object Detection in Point Clouds. In *ECCV*.
- Yongbin Sun, Yue Wang, Ziwei Liu, Joshua E Siegel, and Sanjay E. Sarma. 2020. PointGrow: Autoregressively Learned Point Cloud Generation with Self-Attention. In *WACV*.
- Jiaxiang Tang, Zhaoxi Chen, Xiaokang Chen, Tengfei Wang, Gang Zeng, and Ziwei Liu. 2024a. LGM: Large Multi-View Gaussian Model for High-Resolution 3D Content Creation. *arXiv preprint arXiv:2402.05054* (2024).
- Jiaxiang Tang, Zhaoshuo Li, Zekun Hao, Xian Liu, Gang Zeng, Ming-Yu Liu, and Qingsheng Zhang. 2024b. EdgeRunner: Auto-regressive Auto-encoder for Artistic Mesh Generation. *arXiv preprint arXiv:2409.18114* (2024).
- Keyu Tian, Yi Jiang, Zehuan Yuan, Bingyue Peng, and Liwei Wang. 2024. Visual Autoregressive Modeling: Scalable Image Generation via Next-Scale Prediction. In *NeurIPS*.
- Hugo Touvron, Thibaut Lavril, Gautier Izacard, Xavier Martinet, Marie-Anne Lachaux, Timothée Lacroix, Baptiste Rozière, Naman Goyal, Eric Hambro, Faisal Azhar, et al. 2023. Llama: Open and efficient foundation language models. *arXiv preprint arXiv:2302.13971* (2023).
- Aaron van den Oord, Oriol Vinyals, and Koray Kavukcuoglu. 2017. Neural Discrete Representation Learning. In *NeurIPS*.
- Ashish Vaswani, Noam Shazeer, Niki Parmar, Jakob Uszkoreit, Llion Jones, Aidan N Gomez, Łukasz Kaiser, and Illia Polosukhin. 2017. Attention is all you need. In *NeurIPS*.
- Peng-Shuai Wang. 2023. OctFormer: Octree-based Transformers for 3D Point Clouds. *ACM Trans. Graph. (SIGGRAPH)* 42, 4 (2023).
- Peng-Shuai Wang, Yang Liu, Yu-Xiao Guo, Chun-Yu Sun, and Xin Tong. 2017. O-CNN: Octree-based convolutional neural networks for 3D shape analysis. *ACM Trans. Graph. (SIGGRAPH)* 36, 4 (2017).
- Peng-Shuai Wang, Yang Liu, and Xin Tong. 2022. Dual Octree Graph Networks for Learning Adaptive Volumetric Shape Representations. *ACM Trans. Graph. (SIGGRAPH)* 41, 4 (2022).
- Peng-Shuai Wang, Chun-Yu Sun, Yang Liu, and Xin Tong. 2018. Adaptive O-CNN: A patch-based deep representation of 3D shapes. *ACM Trans. Graph. (SIGGRAPH ASIA)* 37, 6 (2018).
- Xinpeng Wang, Chandan Yeshwanth, and Matthias Nießner. 2021. SceneFormer: Indoor scene generation with transformers. In *3DV*.
- Xinlong Wang, Xiaosong Zhang, Zhengxiong Luo, Quan Sun, Yufeng Cui, Jinsheng Wang, Fan Zhang, Yueze Wang, Zhen Li, Qiying Yu, et al. 2024b. Emu3: Next-token prediction is all you need. *arXiv preprint arXiv:2409.18869* (2024).
- Zhengyi Wang, Jonathan Lorraine, Yikai Wang, Hang Su, Jun Zhu, Sanja Fidler, and Xiaohui Zeng. 2024a. LLaMA-Mesh: Unifying 3D Mesh Generation with Language Models. *arXiv preprint arXiv:2411.09595* (2024).
- Jason Wei, Xuezhi Wang, Dale Schuurmans, Maarten Bosma, Fei Xia, Ed Chi, Quoc V Le, Denny Zhou, et al. 2022. Chain-of-thought prompting elicits reasoning in large language models. In *NeurIPS*.
- Haohan Weng, Zibo Zhao, Biwen Lei, Xianghui Yang, Jian Liu, Zeqiang Lai, Zhuo Chen, Yuhong Liu, Jie Jiang, Chunchao Guo, Tong Zhang, Shenghua Gao, and C. L. Philip Chen. 2024. Scaling Mesh Generation via Compressive Tokenization. *arXiv preprint arXiv:2411.07025* (2024).
- Jiajun Wu, Chengkai Zhang, Tianfan Xue, William T. Freeman, and Joshua B. Tenenbaum. 2016. Learning a probabilistic latent space of object shapes via 3D generative-adversarial modeling. In *NeurIPS*.
- Xiaoyang Wu, Li Jiang, Peng-Shuai Wang, Zhijian Liu, Xihui Liu, Yu Qiao, Wanli Ouyang, Tong He, and Hengshuang Zhao. 2024. Point Transformer V3: Simpler Faster Stronger. In *CVPR*.
- Xiaoyang Wu, Yixing Lao, Li Jiang, Xihui Liu, and Hengshuang Zhao. 2022. Point Transformer V2: Grouped Vector Attention and Partition-based Pooling. In *NeurIPS*.
- Jianfeng Xiang, Zelong Lv, Sicheng Xu, Yu Deng, Ruicheng Wang, Bowen Zhang, Dong Chen, Xin Tong, and Jialong Yang. 2024. Structured 3D Latents for Scalable and Versatile 3D Generation. *arXiv preprint arXiv:2412.01506* (2024).
- Bojun Xiong, Jialun Liu, Jiakui Hu, Chenming Wu, Jinbo Wu, Xing Liu, Chen Zhao, Errui Ding, and Zhouhui Lian. 2024a. TextGaussian: Generating High-quality PBR Material via Octree-based 3D Gaussian Splatting. *arXiv preprint arXiv:2411.19654* (2024).
- Bojun Xiong, Si-Tong Wei, Xin-Yang Zheng, Yan-Pei Cao, Zhouhui Lian, and Peng-Shuai Wang. 2024b. OctFusion: Octree-based Diffusion Models for 3D Shape Generation. *arXiv preprint arXiv:2408.14732* (2024).
- Xingguang Yan, Liqiang Lin, Niloy J. Mitra, Dani Lischinski, Daniel Cohen-Or, and Hui Huang. 2022. ShapeFormer: Transformer-based shape completion via sparse representation. In *CVPR*.
- Yu-Qi Yang, Yu-Xiao Guo, Jian-Yu Xiong, Yang Liu, Hao Pan, Peng-Shuai Wang, Xin Tong, and Baining Guo. 2024. Swin3D: A pretrained transformer backbone for 3D indoor scene understanding. *Comput. Vis. Media* (2024).
- Xumin Yu, Lulu Tang, Yongming Rao, Tiejun Huang, Jie Zhou, and Jiwen Lu. 2022. Point-BERT: Pre-training 3D point cloud transformers with masked point modeling. In *CVPR*.
- Xiaohui Zeng, Arash Vahdat, Francis Williams, Zan Gojcic, Or Litany, Sanja Fidler, and Karsten Kreis. 2022. LION: Latent Point Diffusion Models for 3D Shape Generation. In *NeurIPS*.
- Bowen Zhang, Yiji Cheng, Jialong Yang, Chunyu Wang, Feng Zhao, Yansong Tang, Dong Chen, and Baining Guo. 2024a. GaussianCube: Structuring Gaussian Splatting using Optimal Transport for 3D Generative Modeling. *arXiv preprint arXiv:2403.19655* (2024).
- Biao Zhang, Matthias Nießner, and Peter Wonka. 2022. 3DILG: Irregular latent grids for 3D generative modeling. In *NeurIPS*.
- Biao Zhang, Jiapeng Tang, Matthias Niessner, and Peter Wonka. 2023. 3DShape2VecSet: A 3D shape representation for neural fields and generative diffusion models. *ACM Trans. Graph. (SIGGRAPH)* (2023).
- Jinzhi Zhang, Feng Xiong, and Mu Xu. 2024c. 3D representation in 512-Byte: Variational tokenizer is the key for autoregressive 3D generation. *arXiv preprint arXiv:2412.02202* (2024).
- Jinzhi Zhang, Feng Xiong, and Mu Xu. 2024d. G3PT: Unleash the power of autoregressive modeling in 3D generation via cross-scale querying transformer. *arXiv preprint arXiv:2409.06322* (2024).
- Longwen Zhang, Ziyu Wang, Qixuan Zhang, Qiwei Qiu, Anqi Pang, Haoran Jiang, Wei Yang, Lan Xu, and Jingyi Yu. 2024b. CLAY: A Controllable Large-scale Generative Model for Creating High-quality 3D Assets. *ACM Trans. Graph. (SIGGRAPH)* 43, 4 (2024).
- Hengshuang Zhao, Li Jiang, Jiaya Jia, Philip Torr, and Vladlen Koltun. 2021. Point transformer. In *ICCV*.
- Yue Zhao, Yuanjun Xiong, and Philipp Krähenbühl. 2024. Image and Video Tokenization with Binary Spherical Quantization. *arXiv preprint arXiv:2406.07548* (2024).
- Xin-Yang Zheng, Yang Liu, Peng-Shuai Wang, and Xin Tong. 2022. SDF-StyleGAN: Implicit SDF-Based StyleGAN for 3D Shape Generation. *Comput. Graph. Forum (SGP)* (2022).
- Xin-Yang Zheng, Hao Pan, Peng-Shuai Wang, Xin Tong, Yang Liu, and Heung-Yeung Shum. 2023. Locally Attentional SDF Diffusion for Controllable 3D Shape Generation. *ACM Trans. Graph. (SIGGRAPH)* 42, 4 (2023).
- Kun Zhou, Minmin Gong, Xin Huang, and Baining Guo. 2011. Data-parallel octrees for surface reconstruction. *IEEE. T. Vis. Comput. Gr* 17, 5 (2011).

Received January 2025; accepted March 2025; final version April 2025

## A APPENDIX

*Datasets.* For comparison, we follow the setup from previous works [Zheng et al. 2023] using five categories from ShapeNet with the same data splitting. These categories include *chair*, *table*, *airplane*, *car*, and *rifle*. For meshes in ShapeNet, we first repair meshes and generate SDFs using the method from [Wang et al. 2022]. We then sample 100k points with oriented normals from the resulting mesh surfaces to construct octrees and 200k SDF values for training the VQVAE. For experiments on Objaverse [Deitke et al. 2023], we follow the same data processing pipeline, selecting a subset of 45k meshes using the data splitting provided by [Tang et al. 2024a]. Additionally, we use Cap3D [Luo et al. 2023] for text captioning in the dataset.

*Implementation Details.* To train our VQVAE, we construct octrees with depth 8, corresponding to a resolution of  $256^3$ . The encoder downsamples the input octrees to depth 6 and encodes the features into 32-bit binary tokens at the leaf nodes. The decoder then upsamples the octree back to depth 8. The AdamW optimizer [Loshchilov and Hutter 2019] is used with an initial learning rate of  $1 \times 10^{-3}$ , which linearly decays to  $1 \times 10^{-5}$  throughout training. The VQVAE is trained for 200 epochs on 4 NVIDIA 4090 GPUs, taking approximately 5 days. For training OctGPT, we use the AdamW optimizer with a constant learning rate of  $5 \times 10^{-5}$ . Our model has 170M parameters for ShapeNet dataset, trained on 4 NVIDIA 4090 GPUs for 3 days, and has 440M parameters for Objaverse, trained on 8 NVIDIA 4090 GPUs for 7 days, respectively. During inference, the number of sampling iterations increases from 64 to 256, while the temperature decreases from 1.5 to 0.5 as the octree depth progresses from depth 3 to 6. We use the shading-image-based Fréchet Inception Distance (FID) to evaluate the quality of generated shapes, as proposed in [Zheng et al. 2023]. Specifically, we render the generated meshes from 20 pre-determined viewpoints and calculate the FID between the rendered images and the ground-truth images from the training dataset. A lower FID indicates better quality and diversity of the generated shapes.

*More Comparisons.* After VQVAE training, OctGPT adopts an end-to-end architecture for high-resolution generation without relying on cascaded stages or auxiliary models, thereby reducing implementation complexity and mitigating error accumulation. In contrast,

OctFusion requires a two-stage pipeline even after VQVAE training, and XCube relies on a four-stage architecture with significantly more parameters (1.6B) compared to OctGPT (170M). This unified design allows OctGPT to seamlessly handle complex shape generation. We present comparisons with OctFusion on text-conditioned generation using the Objaverse dataset, as shown in Table 3. We further compare the efficiency and convergence speed of OctGPT with state-of-the-art autoregressive models, including AutoSDF, 3DILG, and MeshGPT, as illustrated in Table 4 and Table 5.

*More Results.* We present more text-conditioned generation results on Objaverse dataset, as illustrated in Fig. 18.

Table 3. The quantitative comparison of *shading-image-based FID* with OctFusion for text-condition experiment on the Objaverse dataset.

Method	FID (Inception)	FID (CLIP-ViT)
OctFusion	81.25	9.09
OctGPT	<b>59.91</b>	<b>6.45</b>

Table 4. Comparisons of efficiency with state-of-the-art 3D autoregressive models. We compare the training iteration time (in seconds) for longer sequences.

Method	5K	10K	20K	40K	80K	160K
AutoSDF	0.4	OOM				
3DILG	0.7	2.0	6.4	22.7	84.8	OOM
MeshGPT	0.3	1.3	4.5	OOM		
OctGPT	0.3	0.4	0.7	1.3	2.5	5.2

Table 5. Comparisons of convergence speed with state-of-the-art 3D autoregressive models. We present the number of parameters, epochs and GPUs

Method	Params	Epochs	GPUs
AutoSDF	32M	400	N/A
3DILG	316M	400	4×A100
MeshGPT	213M	2000	4×A100
OctGPT	170M	200	4×4090

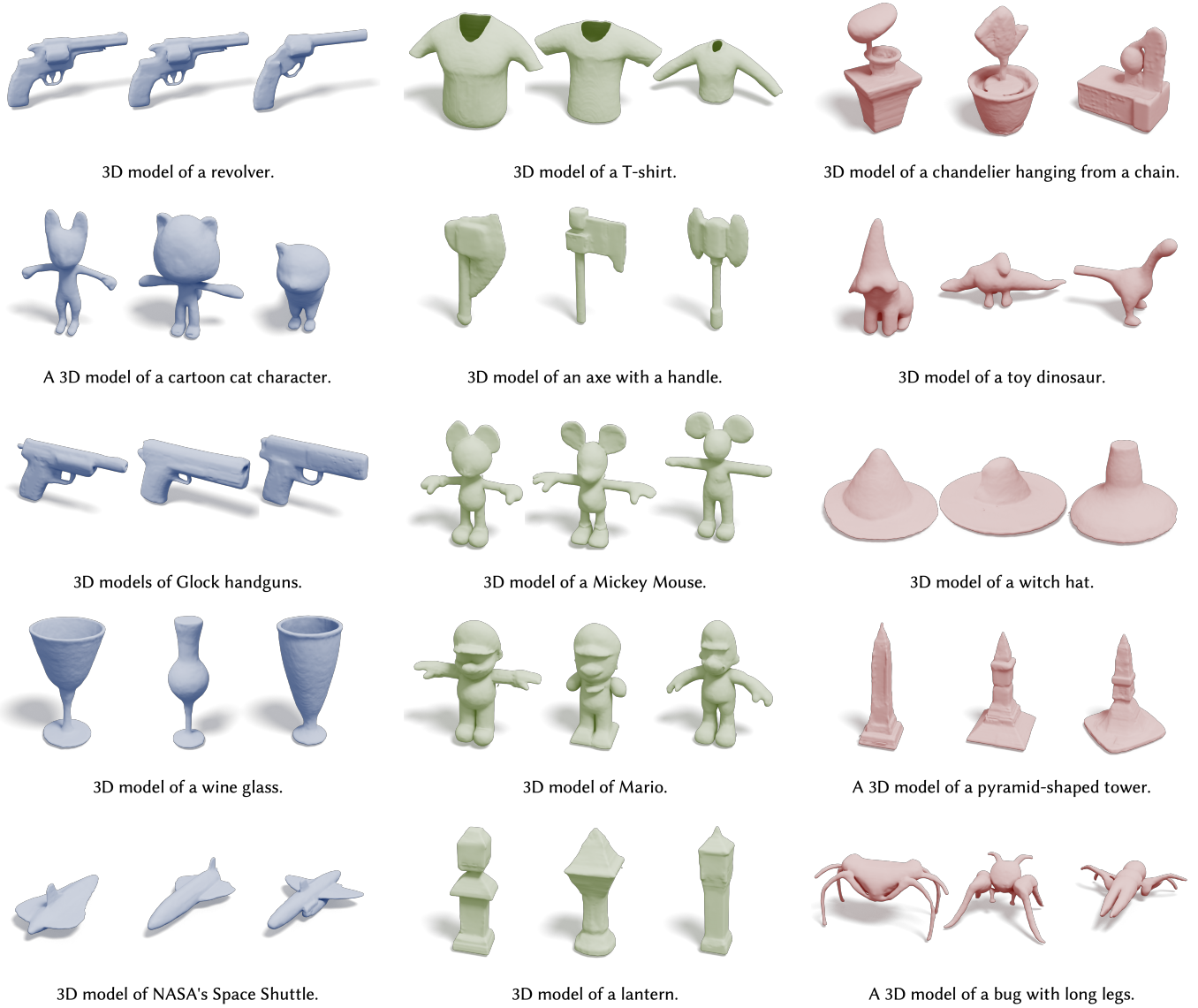


Fig. 18. More text-conditioned generation results on Objaverse dataset.